# AD-A234 523

## TATION PAGE

| 1. AGENCY USE ONLY (Leave blank) | 2. REPORT DATE | 3. REPORT TYPE AND DATES COVERED |
|---|---|---|
| | | Reprint |

**4. TITLE AND SUBTITLE**

Studies of Velocity Fluctuations in the Lower Atmosphere Using the Using the Radar. Part I: Azimuthal Anisotropy

**5. FUNDING NUMBERS**

61102F    2310/A1

**6. AUTHOR(S)**

T. E. Vanzandt, S. A. Smith, T. Tsuda, D. C. Fritts,
T. Sato, S. Fukao, and S. Kato

**7. PERFORMING ORGANIZATION NAME(S) AND ADDRESS(ES)**

University of Alaska
Geophysical Institute
Fairbanks, AK  99775-0800

**8. PERFORMING ORGANIZATION REPORT NUMBER**

AFOSR-TR·  91  0356

**9. SPONSORING / MONITORING AGENCY NAME(S) AND ADDRESS(ES)**

AFOSR/NC    BICI 410
Bolling AFB, DC  20332-6448

**10. SPONSORING / MONITORING AGENCY REPORT NUMBER**

F49620-87-C-0024
AFOSR-86-0050

**11. SUPPLEMENTARY NOTES**

**12a. DISTRIBUTION / AVAILABILITY STATEMENT**

Approved for public release; distribution is unlimited

**12b. DISTRIBUTION CODE**

**13. ABSTRACT (Maximum 200 words)**

We present in this paper a study of the azimuthal anisotropy of the motion field observed during a six-day campaign in March 1986 using the MU radar in Shigaraki, Japan. The radial wind velocity was observed at $20°$ zenith angle, at every $30°$ of azimuth during four days, and at every $45°$ during two days. A jet stream was present during the entire six days. The average radial velocity variance from 10.4 to 19.2 km was calculated every four minutes and then averaged over 20 minutes or one hour.

The average variance was found to be a strong function of both azimuth and time. The azimuthal variations were analyzed in terms of the mean and the first and second harmonics. The mean is proportional to the kinetic energy per unit mass of the radial wind fluctuations, and the first harmonic is proportional to the vertical flux of horizontal momentum per unit mass. The strong azimuthal variation was usually dominated by the second harmonic; i.e., with two peaks, but was occasionally dominated by the first harmonic, with one peak. The phase of the first harmonic was usually westward, but the phase of the second harmonic was quite variable.

It was shown by a development of gravity wave theory that all of the observed azimuthal variations could probably be caused by a gravity wave field whose parameters vary with time.

**14. SUBJECT TERMS**

91 4 16 148

**15. NUMBER OF PAGES**

12

**16. PRICE CODE**

| 17. SECURITY CLASSIFICATION OF REPORT | 18. SECURITY CLASSIFICATION OF THIS PAGE | 19. SECURITY CLASSIFICATION OF ABSTRACT | 20. LIMITATION OF ABSTRACT |
|---|---|---|---|

# Studies of Velocity Fluctuations in the Lower Atmosphere Using the MU Radar.
## Part I: Azimuthal Anisotropy

T. E. VANZANDT,* S. A. SMITH,**,@ T. TSUDA,† D. C. FRITTS,†† T. SATO,† S. FUKAO† AND S. KATO†

*Aeronomy Laboratory, National Oceanic and Atmospheric Administration, Boulder, Colorado
**NASA/Marshall Space Flight Center, Huntsville, Alabama
†Radio Atmospheric Science Center, Kyoto University, Uji, Kyoto, Japan
††Geophysical Institute, University of Alaska, Fairbanks, Alaska

(Manuscript received 11 August 1988, in final form 17 May 1989)

### ABSTRACT

We present in this paper a study of the azimuthal anisotropy of the motion field observed during a six-day campaign in March 1986 using the MU radar in Shigaraki, Japan. The radial wind velocity was observed at 20° zenith angle, at every 30° of azimuth during four days, and at every 45° during two days. A jet stream was present during the entire six days. The average radial velocity variance from 10.4 to 19.2 km was calculated every four minutes and then averaged over 20 minutes or one hour.

The average variance was found to be a strong function of both azimuth and time. The azimuthal variations were analyzed in terms of the mean and the first and second harmonics. The mean is proportional to the kinetic energy per unit mass of the radial wind fluctuations, and the first harmonic is proportional to the vertical flux of horizontal momentum per unit mass. The strong azimuthal variation was usually dominated by the second harmonic; i.e., with two peaks, but was occasionally dominated by the first harmonic, with one peak. The phase of the first harmonic was usually westward, but the phase of the second harmonic was quite variable.

It was shown by a development of gravity wave theory that all of the observed azimuthal variations could probably be caused by a gravity wave field whose parameters vary with time.

## 1. Introduction

Atmospheric parameters are observed to fluctuate on all scales. When these fluctuations are approximately sinusoidal, they can be interpreted as being due to waves, which in the mesoscale are almost certainly internal gravity waves. However, the fluctuations are sometimes not sinusoidal, so that their cause is not immediately evident. Dewan (1979) and VanZandt (1982) suggested that the mesoscale fluctuations are due to a random superposition of gravity waves, in analogy with the internal gravity wave model successfully applied to very similar fluctuations in the ocean (Garrett and Munk 1972, 1975). Gage (1979), on the other hand, suggested that the mesoscale fluctuations were due to the energy spectrum of two-dimensional turbulence (a limiting case of stratified turbulence).

The dynamics of these processes and their dynamical effects on the atmosphere are quite different. In the gravity wave field the energy is thought to cascade toward small scales, where the waves break down, with at least part of their energy dissipating into inertial-

range turbulence. On the other hand, in stratified turbulence the energy cascades from smaller toward larger scales. Other important differences are that gravity waves propagate away from the region of their generation, so that they may have significant vertical fluxes of energy and momentum, which, in regions of wave dissipation, can cause large mean-flow accelerations and turbulence intensities (Vincent and Reid 1983; Fritts and Vincent 1987; Reid and Vincent 1987). These effects are now understood to be important for global atmospheric dynamics and structure (Houghton 1978; Lindzen 1981; Fritts 1984; Palmer et al. 1986).

It is thus quite important to describe the mesoscale fluctuations, to understand their dominant dynamical processes, and to assess their effects on the atmosphere. This paper is the first of two papers in which we examine some of the characteristics of the mesoscale motion field in the troposphere and lower stratosphere, utilizing the unique capabilities of the MU radar in Shigaraki, Japan. The MU radar can sound in up to 16 different directions essentially simultaneously, which permits the conduct of experiments that would be impossible using any other radar. We have taken advantage of this capability to measure the radial velocity as a function of azimuth during a six-day campaign in March 1986. These data are used in this paper to study the azimuthal anisotropy of the variance of radial velocity. Although the azimuthal anisotropy of

---

@ A Universities Space Research Association Visiting Scientist.

Corresponding author address: Dr. T. E. VanZandt, NOAA/ERL, Aeronomy Laboratory, 325 Broadway, Boulder, CO 80303.

the mesoscale fluctuations has been studied in the mesosphere (Meek et al. 1985; Ebel et al. 1987; Vincent and Fritts 1987; Manson and Meek 1988), this is apparently the first study in the lower atmosphere. The companion paper by Fritts et al. (1989) studies the vertical flux of horizontal momentum and other properties of the motion field.

In section 2 the experimental configuration and basic data are described in considerable detail; only a brief description is given in the second paper. The background wind and temperature structure during our experiment are presented in section 3, and the variations of the variance of the radial velocity versus azimuth and time are described in section 4. In section 5 a model is developed for the azimuthal anisotropy of the variance due to a gravity wave field, and it is shown that probably all of the observed variations could be explained by a time-dependent gravity wave field. Conclusions are presented in section 6.

## 2. Experimental configuration and velocity data

The experiment was conducted using the MU radar, located at 34.85°N, 136.10°E, 370 m MSL, in Shiga prefecture, Japan. The relief in this region is strong, with peaks up to 800 m within 10 km and up to 1200 m within 30 km. The MU radar is a monostatic pulsed Doppler radar, operating at a frequency of 46.5 MHz (wavelength 6.45 m). The antenna is circular with a diameter of 103 m, resulting in a two-way, half-power beamwidth of 2.5°. Further details about the MU radar can be found in Fukao et al. (1985).

The present experiment was conducted from 1122 JST (Japan Standard Time; =UTC + 9 h) 8 March 1986, until 1549 JST 14 March 1986 with only minor interruptions, for a total of 6 d, 4.5 h. During the first four days, 12 beams were directed at a zenith angle $\chi$ = 20° at azimuths $\theta$ in steps of 30°, and four beams were at $\chi$ = 10° at $\theta$ in steps of 90°. During the last two days, 8 beams were at $\chi$ = 20° at $\theta$ in steps of 45°, and one beam was directed at the zenith. However, the studies in the present three papers used only the beams at $\chi$ = 20°, whose configuration is shown in Fig. 1.

The pulse length was 300 m and the range gates were centered at ranges from 7.5 km to 20.4 km in steps of 300 m; at $\chi$ = 20° the range gates were centered at heights above ground from 7.05 to 19.17 km and at altitudes above sea level from 7.42 to 19.54 km in steps of 282 m. The average time resolution of the data used in our analyses was 237 s (4 min), with 2256 records.

## 3. Basic data and meteorological parameters

Daily profiles of the zonal and meridional components of the background horizontal wind were determined from the radar radial wind measurements as follows. The zonal component at each altitude and time was determined by first averaging the radial wind mea-
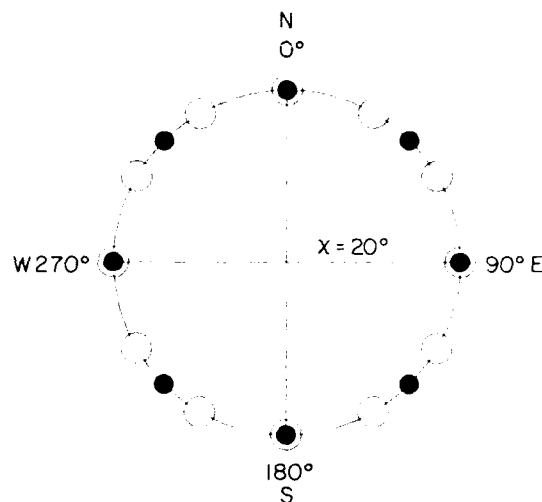


FIG. 1. Configuration of the radar beams used in this study. All beams used were at a zenith angle $\chi$ = 20°. The beams at positions indicated by open and closed circles were used during the first four days and the last two days of the experiment, respectively.

sured in the 90° and 270° azimuths, averaging the result over each successive 24-hour period centered at 2322 JST, smoothing the resulting profile with a low-pass filter with a cutoff at 3 km in order to avoid contamination by waves with short vertical wavelengths and low frequencies, and finally multiplying by $1/\sin 20°$ = 2.92 to obtain the horizontal component. The meridional wind was calculated in the same way. The resulting zonal and meridional wind profiles, positive toward the east and north, are shown in the left and right panels of Fig. 2a, with the zero wind for each day displaced to the right by 14.6 m s⁻¹.

A zonal jet stream was present during the entire six-day period, with a peak zonal wind of 35 m s⁻¹ at about 15 km on the first day, increasing to 58 m s⁻¹ at about 12.5 km on the third day, and then decreasing to 48 m s⁻¹ at 10 to 12 km on the sixth day. Below the jet stream the changes were much larger; at 10 km the horizontal wind speed increased from about 4 m s⁻¹ on the first day, to 50 m s⁻¹ on the third day, and then decreased only slightly. As a result, the jet stream became much broader on its lower side.

The background temperature profile in Fig. 2b was derived from routine radiosonde ascents at 0000 and 1200 UTC (0900 and 2100 JST) from Shionomisaki, 100 km south of the MU radar. The reported temperatures were interpolated to 1000 m intervals, averaged over the entire six-day period, and then smoothed with the same low-pass filter as the wind profiles. The background profile of $N^2$ (where $N$ is the buoyancy frequency), also shown in Fig. 2b, was determined by differencing the mean temperature profile over 2000 m.

The altitude of the tropopause determined from each radiosonde ascent increased from about 10.5 km on the first two days to about 12 km on the last day, with an average of about 11 km.
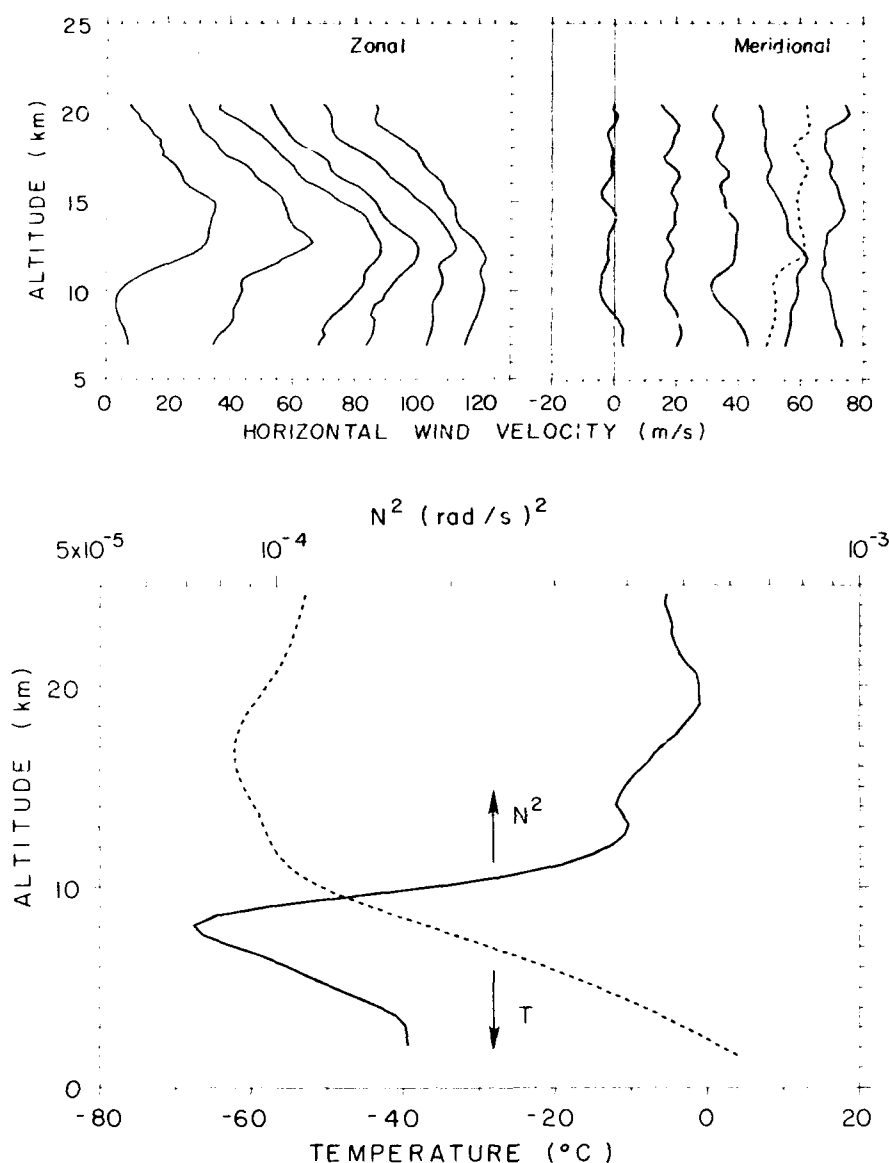
FIG. 2. (a) Profiles of background zonal and meridional horizontal wind averaged over 24 h centered on 2322 JST 8–12 March 1986. The zero wind for each day is displaced to the right by 14.6 m s$^{-1}$. (b) Profiles of temperature $T$ and buoyancy frequency squared $N^2$ averaged over the entire six-day period.

Figure 3 shows the inverse Richardson number $Ri^{-1}$ $= S^2/N^2$. Here $S$ is the magnitude of the vector shear calculated from wind profiles averaged over 1 h and differenced over 300 m of range, so that each box in Fig. 3 is 1 h long and 282 m high, and $N^2$ is the mean over the entire six-day period from Fig. 2b. The boxes are coded as follows: black, $Ri^{-1} > 1$; open, $1 > Ri^{-1}$ $> \frac{1}{3}$; blank, $\frac{1}{3} > Ri^{-1}$. The zero time on this and succeeding figures is the beginning time of our experiment, 1122 JST 8 March. Since $N^2$ is a mean, the variations of $Ri^{-1}$ with time must be due entirely to variations of $S^2$. The region of generally large $Ri^{-1}$ in the lower stratosphere between about 10 and 12 km was caused

by the large shears on the bottom of the jet stream, which diminished during the six-day period (see Fig. 2a). On the top of the jet stream the shears were much smaller and $N^2$ was larger so that $Ri^{-1}$ was considerably smaller.

The richness and variability of the radial velocity data measured by the MU radar are illustrated by Figs. 4 and 5, which show time series of low-pass and high-pass filtered data, respectively. The 3 db cutoff was set at a period of 33 h to ensure that gravity wave motions near the inertial period (20.95 h at the 34.85° latitude of the MU radar) were not attenuated in the high-pass time series and did not contaminate the low-pass series.
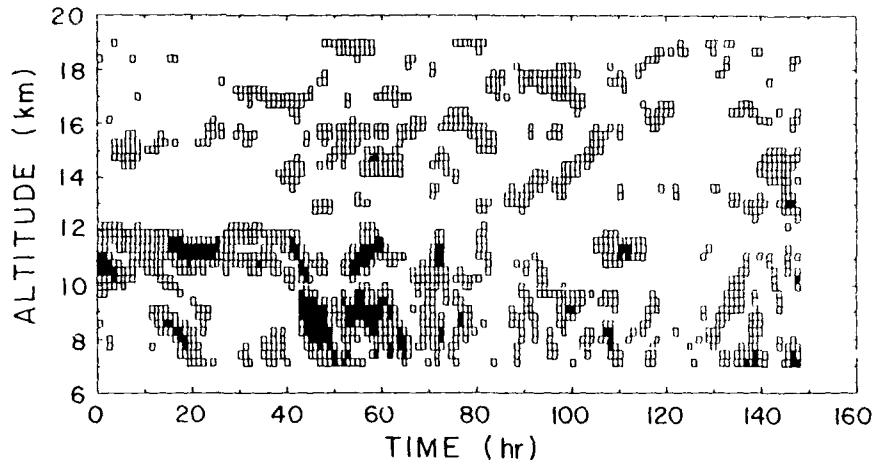
FIG. 3. The inverse Richardson number $Ri^{-1} = N^2/S^2$ versus time and altitude. Here $N^2$ is from Fig. 2b and $S^2$, the vertical shear squared, is derived from the wind profiles measured by the radar. Each box is 1 h wide and 282 m high. The boxes are coded as follows: black, $Ri^{-1} > 1$; open, $1 > Ri^{-1} > \frac{1}{3}$; blank, $\frac{1}{3} > Ri^{-1}$.

In each figure, panels (a) and (b) present the radial velocity measured by the 90° (eastward) and 0° (northward) beams, respectively. The velocity scale on the ordinate is for the lowest range gate at an altitude of 7.42 km and each successive curve is for 282 m higher and is shifted upward by 2 m s$^{-1}$ in Fig. 4 and by 3 m s$^{-1}$ in Fig. 5.

In the low-pass time series at and below the jet core the zonal flow increased rapidly between about 20 and 60 h while the meridional flow underwent a large oscillation from about 60 to 150 h. Above the jet core both components oscillated with periods of about two days. The high-pass data below the jet core also exhibited considerable variability. Above the jet core the amplitudes decreased and became less organized with increasing height.

## 4. Variance as a function of azimuth and time

The present study of the anisotropy of the fluctuation field is based entirely on the variance of the radial velocity as a function of azimuth and time, which was calculated as follows. At each observation time and altitude the radial wind profiles in the zonal and meridional planes were averaged over 320 records = 21.07 h (about equal to the inertial period) centered on the observation time, and the result was smoothed with a low-pass filter with a cutoff at 3 km. Then the background profile at each azimuth was calculated from the zonal and meridional components. This profile was then subtracted from the observed profile for that azimuth and time, and the profile of variance was calculated.

The fluctuations of the variance can be reduced by averaging over several altitudes and times. In order to treat a reasonably homogeneous region, we have averaged over only the lower stratosphere; i.e., over al-

titudes from 10.43 to 19.17 km (ranges from 11.1 to 20.4 km).

Time series of radial velocity variance at each azimuth averaged over 15 records = 1 h are presented in Fig. 6. The variance varied strongly versus time, with significant peaks at about 42, 57, 70, 81, 90, 109, and 134 h. Most of the time the azimuthal variation was dominated by the second harmonic; this was particularly evident during some of the peaks. The first harmonic was usually much smaller than the second, but occasionally it was larger when the second harmonic was small.

The observed variance versus azimuth in a given time interval can be described succinctly by fitting the mean and first two sinusoidal harmonics by least squares. This description is also convenient for interpretation, since the terms can be interpreted physically. The mean divided by $\sin^2 20°$ is related to the kinetic energy per unit mass of the radial wind fluctuations. According to the analysis of Vincent and Reid (1983), the first harmonic is proportional to the vertical flux of horizontal momentum per unit mass, which has an important effect on global atmospheric dynamics and which is treated in considerable detail in the second paper of this series (Fritts et al. 1990). All three terms can be interpreted in terms of gravity wave theory, as will be shown in section 5.

Four examples of the resulting variance versus azimuth averaged over five records ($\sim 20$ min) and the harmonic fits are shown in Fig. 7. Several features are illustrated. The running mean azimuthal curve centered at record number 640 was dominated by the first harmonic. But at record 645, only 20 minutes later, there was a large second harmonic in addition to a significant first harmonic, as evidenced by the unequal maxima and minima. The very rapid change from records 640 to 645 was at the beginning of the peak at
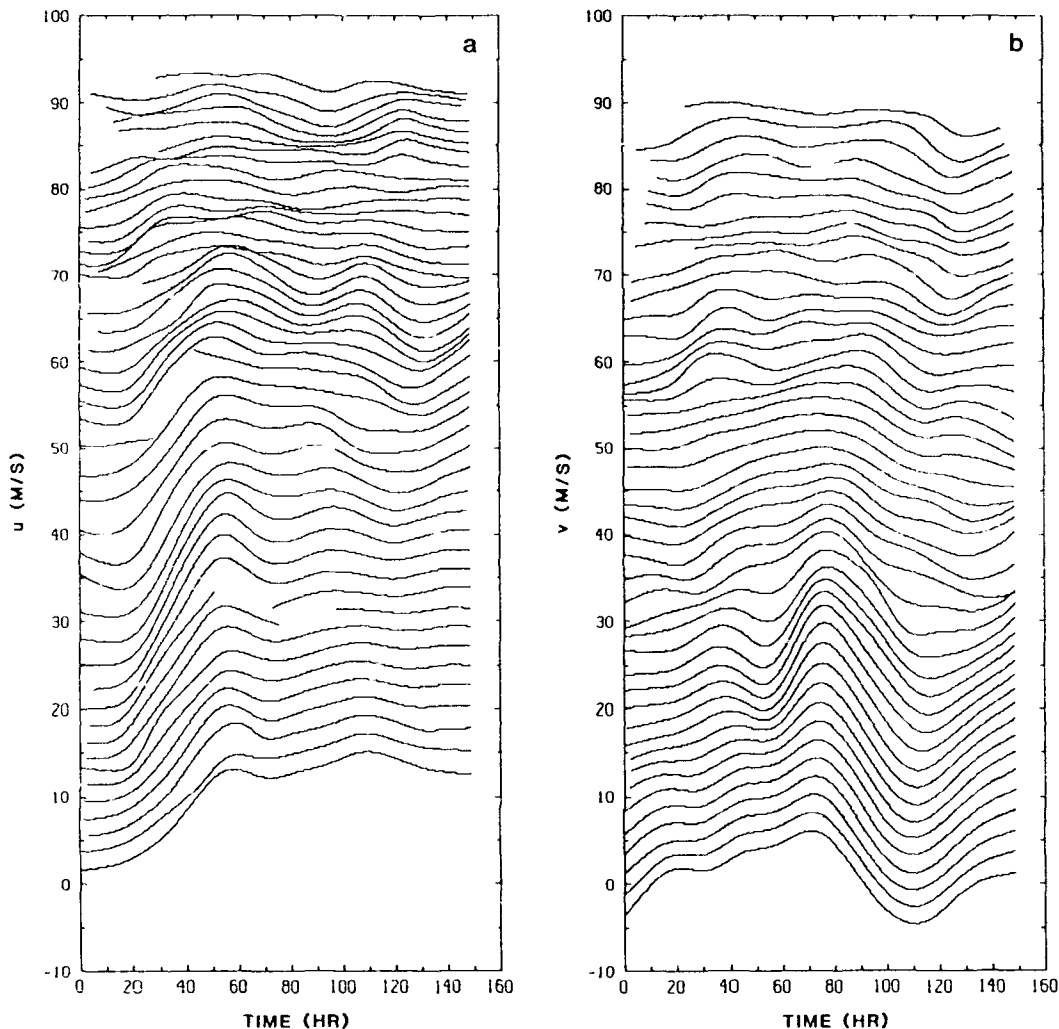
FIG. 4. Low-passed eastward (a) and northward (b) time series of radial velocity with the 3 db cutoff period at 33 h. The radial velocity scale is for the lowest range gate at an altitude of 7.42 km and each successive curve is for 282 m higher and is shifted upward by 2 m s$^{-1}$.

42 h in Fig. 6. Records 660 and 700 were both dominated by the second harmonic, and the first harmonic was small, since the peaks were nearly equal, but the ratio of the second harmonic to the mean was much larger in record 660. Much of this discussion will be devoted to interpretation of the wide variety of azimuthal behaviors.

Figure 8 shows each successive fitted azimuthal curve centered on records 440 to 830 (at times from 29.0 to 80.3 h) with the zero for each successive curve shifted 1 (m s$^{-1}$)$^2$ to the right. The four examples in Fig. 7 are indicated by arrows between 40 and 50 h at the margin of the upper panel. The predominance of the second harmonic, particularly during the peaks at 42, 57 and 70 h is clearly visible. Note also the phase changes during the 42 and 70 h peaks.

These variations are presented quantitatively in Fig. 9. The amplitudes $a_0$ (upper bold curve), $a_1$ (lower bold curve), and $a_2$ (thin curve) of the mean and the

first and second harmonics are shown in panel (a). The corresponding phase angles relative to north of the maxima, $\phi_1$ (bold) and $\phi_2$ (thin), are shown in panel (b). These quantities are running averages over 1 h plotted every 4 min.

From 12 to 30 h, $a_1$ varied with a period of about 2 h, while $\phi_1$ changed by $\pm 90°$ or $180°$ in alternate cycles. Similar periodic variations of $a_1$, without significant phase changes, also occurred later, particularly from 80 to 90 h. After 45 h, $\phi_1$ tended to oscillate about 270°, but there was a tendency for $\phi_1$ to depart from 270° during the maxima of $a_1$. There did not appear to be any overall correlation or relation between the phases $\phi_1$ and $\phi_2$.

## 5. Comparison with gravity wave models

It was pointed out in the Introduction that two different dynamical processes have been proposed to account for mesoscale velocity fluctuations: gravity waves
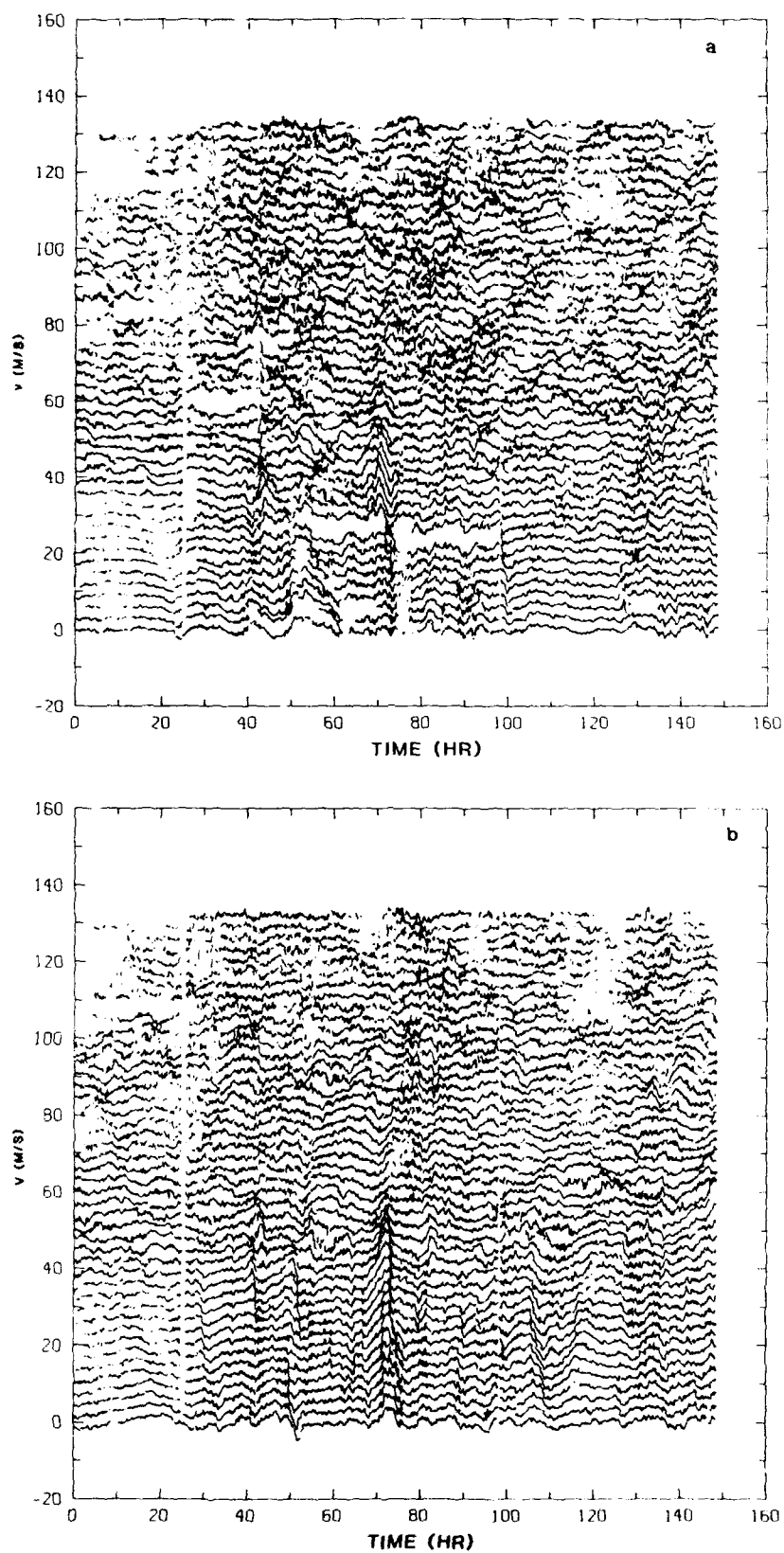
FIG. 5. High-passed eastward (a) and northward (b) time series of radial velocity with the 3 db cutoff period at 33 h. The radial velocity scale is for the lowest curve and successive curves are displaced upward by 3 m s$^{-1}$.
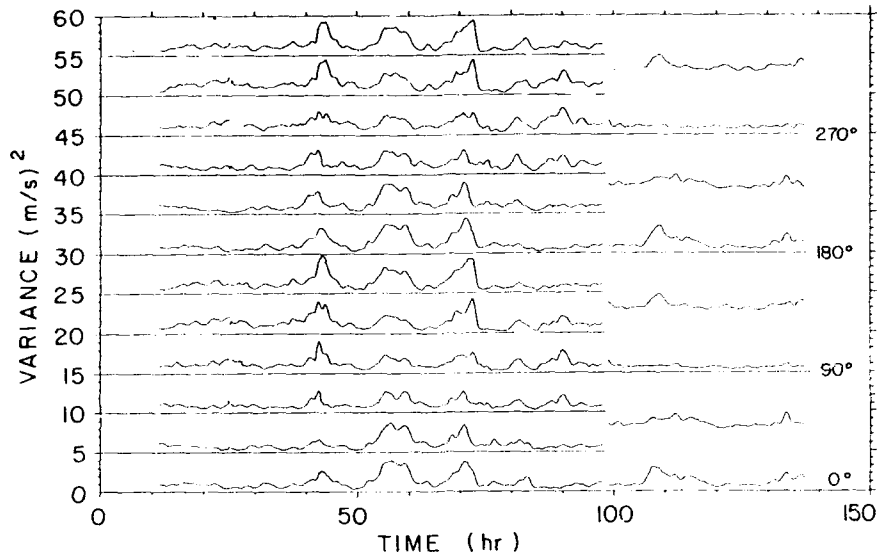
FIG. 6. Variance at each azimuth vs time averaged from 10.4 to 19.2 km and over 1 h. The
lines of data correspond to the beam positions shown in Fig. 1.

and stratified turbulence. Because their effects on the atmosphere are quite different, it is important to evaluate the relative significance of these processes. In this section we consider to what extent the observed fluctuations can be explained in terms of gravity waves. We do this by developing models for the radial variance as a function of azimuth due to gravity waves. We find that probably all of the observed azimuthal curves can be explained by a suitable field of gravity waves. Unfortunately, the theory of stratified turbulence is not nearly as well developed as the theory of gravity waves, so that it is not possible to show whether or not the observed variations could be due to stratified turbulence.
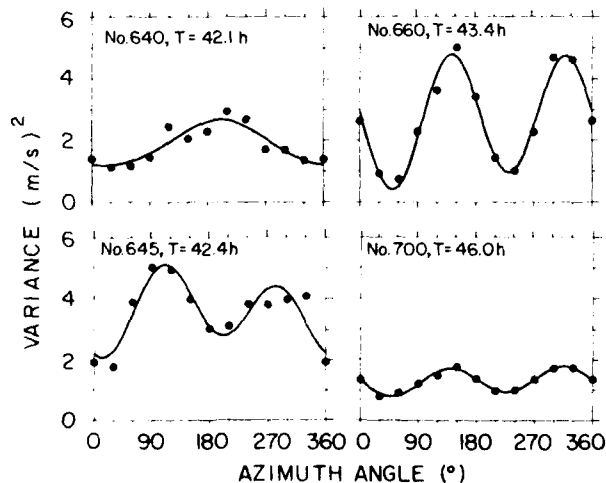


FIG. 7. Examples of the variance versus azimuth. The data points are averaged over five records = 20 min. centered on the labeled record number and time. The curve is the sum of the mean and first and second harmonics fitted to the data points by least squares. Note that the panels labeled 640 and 645 are centered only 20 min apart.

The gravity wave model is developed as follows. First, we develop a model for the radial variance as a function of azimuth due to a gravity wave with a given frequency, wavenumber, and direction of propagation that is sampled over all phases of the wave. Even though this model treats only a single wave and ignores the effects of Doppler shifting due to the background wind, the resulting model curves resemble the observed curves. The model also provides insight into how gravity waves can cause the observed variations. Second, the effect of a broad frequency spectrum is explored by integrating over a power-law spectrum. Third, a more general azimuthal distribution of propagation vectors is considered. Finally, we consider the variance due to quasi-inertial waves that are not sampled over all phases. Although the azimuthal curves from these models resemble the observed curves, we do not attempt actually to fit the model and observed azimuthal curves for reasons that will become apparent.

The azimuthal variation of the variance due to a gravity wave field can be modeled by a slight generalization of the model that VanZandt (1985), following Pinkel (1981), developed for the power spectrum of radial velocity observed by a Doppler radar. The assumptions are the same as those of VanZandt (1985) except as noted. In particular, we have assumed that there is no background wind. For a radar pointing at an azimuth $\theta_R = 0°$ and zenith angle $X$, the observed profile of radial velocity $v_+$ at a range $r$ is given by

$$v_+ = \mathrm{Re}\{(\Theta_1 \sin X \mp \Phi^{-1} \cos X)A(k, \omega, \theta)$$

$$\times \exp[i(kr \sin X \cos\theta \pm mr \cos X - \omega t)]\}  \quad (1)$$

where the upper and lower signs are taken for upward and downward phase propagation (downward and upward group propagation). Here $\Theta_1 = \cos\theta + i(1/\omega)\sin\theta$

and $\Phi^{-1} = (\omega/N)\{[1 - (1/\omega)^2]/[1 - (\omega/N)^2]\}^{1/2}$, where $\omega$ and $N$ are the intrinsic and buoyancy frequency normalized by the inertial frequency, and $A(k, \omega, \theta)$ is the amplitude of the wave. Variables $k$ and $m$ are the horizontal and vertical wavenumbers, and the $\sin\chi$ and $\cos\chi$ terms are the contributions to the radial velocity from the horizontal and vertical velocity components, respectively. Of course, (1) is valid only for $1 \leqslant \omega \leqslant N$.

If we assume that the gravity wave energy spectrum is variables-separable, following Garrett and Munk (1975) and VanZandt (1982), then the spectrum as a function of azimuth $\theta$ is given by

$$F_{r_\pm}(m, \omega, \theta) = (A_\pm/2\pi)EA(m/m_*)B(\omega)\int_\theta d\theta H(\theta) \cdot |(\cos\theta + i\omega^{-1}\sin\theta)\sin\chi \mp \Phi^{-1}\cos\chi|^2 \quad (2)$$

where $A_+$ and $A_-$ ($= 1 - A_+$) are the fractions of energy associated with upward and downward phase propagation, respectively; $E$ is the total energy per unit mass; $A(m/m_*)$ is the wavenumber spectrum, where $m_*$ is the characteristic vertical wavenumber; $B(\omega)$ is the spectrum as a function of normalized intrinsic frequency $\omega$; and $H(\theta)$ is the azimuthal distribution of gravity wave propagation vectors.

For the purpose of discussion we assume that all of the waves are propagating in the azimuth $\theta_H$ so that $H(\theta)/2\pi = \delta(\theta - \theta_H)$, where $\delta$ is the Dirac delta function. Then the integration over $\theta$ replaces $\theta$ by $\theta_H$. But since the radar scans in azimuth, it is more convenient to assume that the azimuth of the radar $\theta_R$ varies and $\theta_H$ is fixed at $0°$, which amounts to the transformation $\theta = \theta_H - \theta_R$ with $\theta_H = 0°$. Then with some rearrangement

$$F_r(\omega, \theta_R) = EB(\omega)\sin^2\chi[\delta_+/2 + C^2\omega^2\delta_-$$
$$+ 2(1 - 2A)C\omega\delta_-^{1/2}\cos\theta_R + (\delta_-/2)\cos2\theta_R], \quad (3)$$

where $\delta_\pm = 1 \pm (1/\omega)^2$ and $C = \cot\chi/N$.

All of the results presented in this paper were calculated for $N = 200$, appropriate to the lower stratosphere at the latitude of the MU radar. Then with $\chi$ = $20°$, $C = 0.0137$. Equation (3), normalized by the mean, is plotted versus $\theta$ in Figs. 10a–c for $A = 1$, $\frac{3}{4}$, and $\frac{1}{2}$, respectively, and for $\omega = 1$, $10^{1/2}$, 10, $10^{3/2}$, $10^2$, and 200. (Note that in Fig. 10c the curves for $\omega = 10^{1/2}$ and $10^{3/2}$ happen to be almost identical.)

The changes in the relative magnitudes of the peaks can be understood as follows. Further insight can be found in, e.g., Hines (1960, 1974), Gossard and Hooke (1975), and Pinkel (1981). For downward phase propagation, the gravity wave motions lie in a plane of constant phase whose direction normal is tilted toward 180° by an angle $\beta = \tan^{-1}(\Phi^{-1})$ ($\approx \omega/N$ for $1 \ll \omega \ll N$). When $\omega = 1$, $10^{1/2}$, 10, $10^{3/2}$, $10^2$, or 200, $\beta = 0°$, $0.86°$, $2.85°$, $9.09°$, $30.0°$, or $90°$, respectively. Thus the phase plane remains nearly horizontal until $\omega \gg 1$. When $\omega = 1$ the motion is circular, so that the variance is the same in all azimuths. But as $\omega$ increases the motion becomes nearly linear along the intersection of the tilted phase plane and the vertical plane $\theta_H = 0°$. Then at $\omega = 200$, where $\beta = 90°$, the variance is again the same in all azimuths.

When the motion is nearly linear, the variance versus $\theta$ is nearly proportional to $\cos^2\psi$, where $\psi$ is the dihedral angle between the radar beam direction and the line of motion (see Fig. 11). At $\theta = 0°$ and 180°, $\cos\psi = \cos(\pi/2 - \chi \pm \beta) = \sin(\chi \mp \beta)$, and at $\theta = 90°$ or
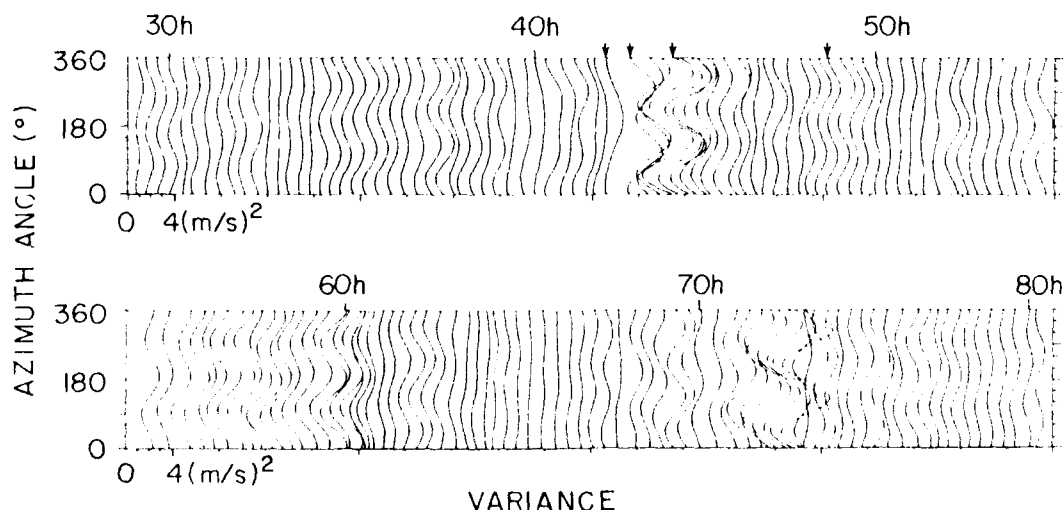


FIG. 8. Successive fitted curves centered 20 min apart from 29.0 to 80.3 h, with the zero for each successive curve shifted to the right by 1 (m s$^{-1}$)$^2$. The four examples shown in Fig. 5 are indicated by arrows in the margin of the upper panel.
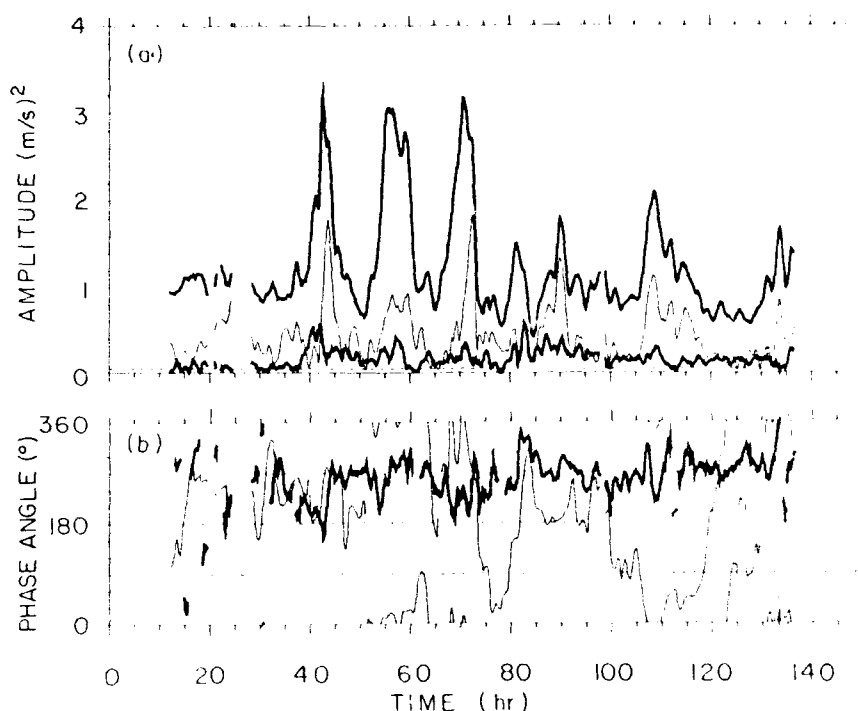
FIG. 9. (a) The amplitudes $a_0$ (upper bold curve), $a_1$ (lower bold curve), and $a_2$ (thin curve) of the mean and the first and second harmonics. (b) The corresponding phase angles $\phi_1$ (bold) and $\phi_2$ (thin) of the maxima relative to north. $\phi_1$ is not plotted when $a_1 < 0.2$. These quantities are running averages over 1 h plotted every 4 min.

$270°$, $\cos\psi = \cos\chi \sin\beta$. When $\omega$ is small and the motions are nearly horizontal, then $\cos\psi \approx \sin\chi$ at $\theta = 0°$ and $180°$, which is much larger than $\cos\psi$ at $\theta = 90°$ and $270°$, so that the variance has two maxima and two minima, as shown in Fig. 10a for $\omega = 10^{1/2}$, 10, and $10^{3/2}$. As $\omega$ increases and the line of motion steepens, $\cos\psi$ at $\theta = 90°$, $180°$, and $270°$ decreases relative to $\theta = 0°$. Indeed, when $\beta = \chi = 20°$ (at $\omega = 68.4$),

$\cos\psi = 0°$; i.e., the motions are normal to the $180°$ beam. Thus, at larger $\omega$ there is only one maximum and one minimum, as shown in Fig. 10a for $\omega = 100$. The westward maximum is consistent with phase surfaces whose normals are tilted toward the east due either to generation by shear instability below the jet stream, or to topographic forcing or convection at lower levels. Of course, upward phase propagation, $A = 0$, 1, 1,
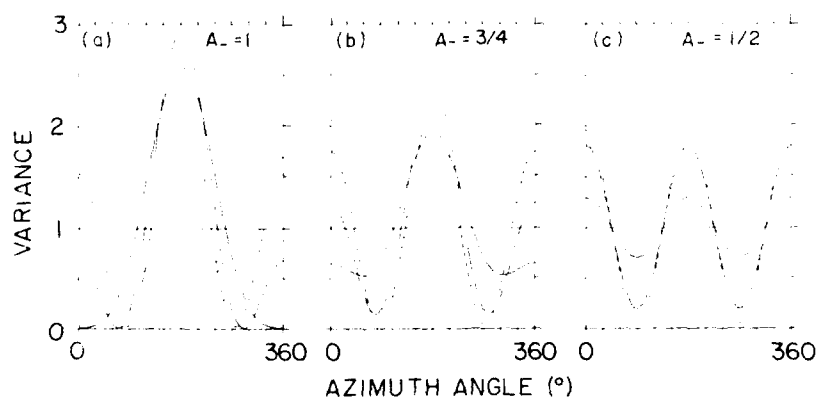


FIG. 10. Radial velocity variance versus radar beam azimuth $\theta$ for a radar beam zenith angle $\chi = 20°$, as a function of gravity wave frequency $\omega$, normalized by the inertial frequency. The frequency code is $\omega = 1$, solid; $10^{1/2}$, dotted; 10, dashed; $10^{3/2}$, dot–dash; 100 and 200, solid. The gravity waves are all assumed to be propagating in the azimuth $0°$, and $A$ is the fraction of the waves with downward phase propagation (upward group propagation). [Note that in panel (c) the curves for $\omega = 10^{1/2}$ and $10^{3/2}$ are almost identical.]
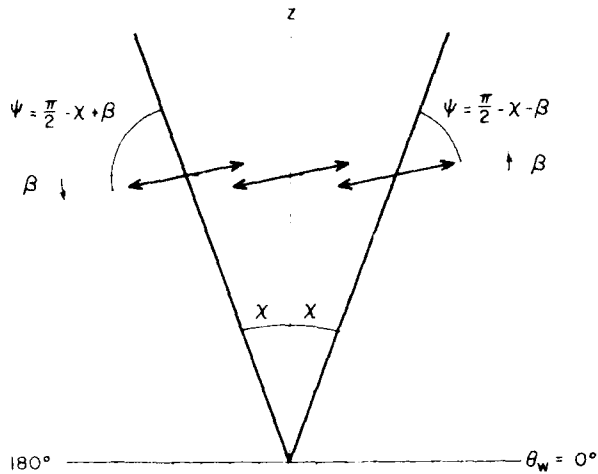
FIG. 11. Sketch illustrating the dihedral angle between radar beams and gravity wave perturbation velocities in the vertical plane of $\theta_w$ = 0° for downward and rightward phase propagation. The double-headed arrows indicate the perturbation motions in three surfaces of constant phase. The sketch is for radar beam zenith angle $\chi$ = 20° and gravity wave frequency $\omega$ = 50, resulting in an inclination angle $\beta$ = 14.5°, and dihedral angles $\psi$ = 55.5° and 84.5°.

produces the same pattern shifted by 180°, so that in Fig. 10c for $A$ = 0.5 the curve between 90° and 270° repeats the curve from 270° to 90°.

The frequency spectra from 24-hour time series of the present dataset, analyzed in the following paper by Fritts et al. (1990), follow a power law $\omega^{-p}$ with $p$ ≈ 5/3. Therefore, (3) has been integrated numerically over all $\omega$ from 1 to 200 (i.e., from the inertial frequency to the buoyancy frequency) with $p$ = 1, 4/3, 5/3, and 2. The resulting curves are shown in Fig. 12.

The curves in Figs. 10 and 12 are symmetrical about $\theta_w$, so that a model with all waves propagating in one direction cannot explain the unequal minima that are often observed in Figs. 7 and 8. In order to demonstrate that a gravity wave model can explain such minima,

Fig. 13 shows the sum of the curve in Fig. 12a for $p$ = 5/3 plus the same curve multiplied by 1/2 and shifted 90° toward the left (counterclockwise).

Of course, in reality the distribution of propagation vectors cannot consist of $\delta$ functions. But the fact that the widths of the maxima and minima in the model curves are similar to the observed widths suggests that the peaks in the actual $H(\theta)$ must indeed be narrow.

The foregoing models assume that the gravity waves in the field are sampled uniformly over all phases, either versus space or time. In the present experiment, averaging over the altitude range of 8.74 km samples over the phase of most waves, since the characteristic vertical wavenumber in the lower stratosphere is only 2–3 km (Fritts et al. 1988). On the other hand, averaging over 20 min in Figs. 7–9 samples over the phase of only waves with short periods. For waves with $\omega$ ≥ 3, where the motion is approximately linear, the partial sampling affects the amplitude, but not the shape of the curves in Figs. 10, 12, and 13. But for waves with $\omega$ ≤ 3, i.e., near the inertial frequency, according to Eq. (1) the perturbation velocity rotates on an ellipse, so that the curves in Fig. 10 also rotate.

The rotations occasionally seen in Fig. 8 may be due to such quasi-inertial waves with long vertical wavelengths. In particular, the counterclockwise rotation just after 70 h could be due to a quasi-inertial wave with a horizontal wavelength of about 1000 km that has been Doppler-shifted to a period of about six hours by the background wind.

It is clear that probably all of the observed curves in Figs. 7 and 8 and the relative amplitudes and phases in Fig. 9a and 9b could be explained by a gravity wave field with suitably chosen time-dependent $B(\omega)$, $H(\theta)$, and $A$. Indeed, it appears that most of the observed curves could be explained by model curves with a frequency spectrum $B(\omega)$ ∝ $\omega^{-5/3}$ with $p$ = 5/3 and appropriate $H(\theta)$ and $A$. There are two kinds of exceptions. First, when $a_1 > a_2$, i.e., when the observed variation is roughly unimodal, $B(\omega)$ must be dominated
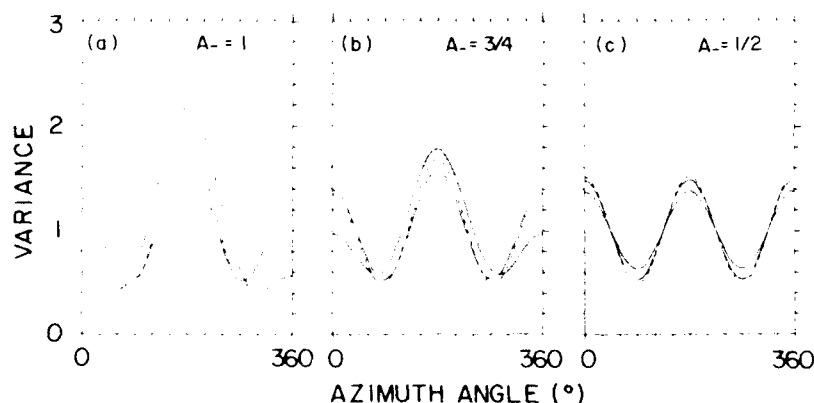


FIG. 12. The curves in Fig. 10 integrated over $\omega$ with frequency spectra $B(\omega)$ ∝ $\omega^{-p}$ with $p$ = 1, solid; 4/3, dotted; 5/3, dashed; and 2, dot–dash. Other parameters are as for Fig. 9.
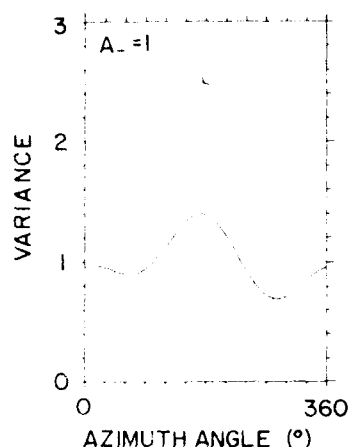
Fig. 13. The sum of the curve in Fig. 12a for $p = \frac{2}{3}$ plus the same curve multiplied by $\frac{1}{2}$ and shifted 90° toward the left. This process generates unequal minima.

by relatively high frequencies and with $A \neq \frac{1}{2}$. Second, during the periods of rotation $B(\omega)$ must be dominated by a quasi-inertial wave.

We have not attempted actually to fit model curves to the observed curves, because the number of parameters is so large that the fittings could not be unique. Moreover, the present model ignores the effects of Doppler shifting due to the background wind, which was quite large during this experiment. Doppler shifting has no effect on the component of motion at right angles to the wind. But in the plane of the wind it changes the shape of the frequency spectrum (Scheffler and Liu 1986; Fritts and VanZandt 1987). For radial spectra it tends to reduce the effective value of $p$. Thus, Doppler shifting would tend to move the model results toward the curves with smaller $p$ in Fig. 12.

## 6. Conclusions

We find that the radial velocity variance averaged from 10.4 to 19.2 km is a strong function of azimuth $\theta$ and time. The azimuthal variations were analyzed in terms of the mean and first and second harmonics. The amplitude $a_0$ of the mean divided by $\sin^2\chi$ is related to the kinetic energy per unit mass. The first harmonic is proportional to the vertical flux of horizontal momentum, which is discussed in the second paper (Fritts et al. 1990) of this series.

Usually, the azimuthal variation was dominated by the second harmonic, but the ratio of the amplitude of the second harmonic to the mean and first harmonic terms was quite variable. When the first harmonic was large enough, it often made the two peaks and the two valleys unequal. Indeed, the first harmonic was occasionally so large that there was only one peak. The phase of the maximum of the first harmonic was usually westward, but the phase of the second harmonic was quite variable.

It was shown by a development of gravity wave theory that probably all of the observed azimuthal variations could be caused by a field of gravity waves. The variations with time must then be due to variations of the parameters of the gravity wave field.

Because the theory of stratified turbulence is not sufficiently well developed, it is not possible to develop model azimuthal curves that can be critically compared with the observed curves. Thus, it cannot be determined to what extent the observed variations may be due to stratified turbulence.

The present observations and conclusions strictly apply only to the conditions under which the observations were made: the observations were made in March in the middle latitudes of east Asia, a jet stream was overhead, and the relief near the MU radar is strong. In order to understand how much our results depend on these particular conditions, similar experiments under other conditions are needed. The effect of background meteorological conditions and season can be studied by the MU radar. The effect of terrain, latitude, etc., can be explored by other radars in different terrains.

REFERENCES

Dewan, E. M., 1979: Stratospheric wave spectra resembling turbulence. *Science,* **204,** 832–835.

Ebel, A., A. H. Mansor and C. F. Meek, 1987: Short-period fluctuations of the horizontal wind measured in the upper atmosphere and possible relations to internal gravity waves. *J. Atmos. Terr. Phys.,* **49,** 385–401.

Fritts, D. C., 1984: Gravity wave saturation in the middle atmosphere. A review of theory and observations. *Rev. Geophys. Space Phys.,* **22,** 275–308.

——, and T. E. VanZandt, 1987: The effects of Doppler shifting on the frequency spectra of atmospheric gravity waves. *J. Geophys. Res.,* **92,** 9723–9732.

——, and R. A. Vincent, 1987: Mesospheric momentum flux studies at Adelaide, Australia: Observations and a gravity wave tidal interaction model. *J. Atmos. Sci.,* **44,** 605–619.

——, T. Tsuda, T. Sato, S. Fukao and S. Kato, 1988: Observational evidence of a saturated gravity wave spectrum in the troposphere and lower stratosphere. *J. Atmos. Sci.,* **45,** 1741–1759.

——, ——, T. E. VanZandt, S. A. Smith, T. Sato, S. Fukao and S. Kato, 1990: Studies of velocity fluctuations in the lower atmosphere using the MU radar. Part II: Momentum fluxes and energy densities. *J. Atmos. Sci.*, **47**, 51–66.

Fukao, S., T. Sato, T. Tsuda, S. Kato, K. Wakasugi and T. Makihira, 1985: The MU radar with an active phased array system: 1. Antenna and power amplifiers, 2. In-house equipment. *Radio Sci.*, **20**, 1155–1176.

Gage, K. S., 1979: Evidence for $k^{5/3}$ power law inertial range in mesoscale two-dimensional turbulence. *J. Atmos. Sci.*, **36**, 1950–1954.

Garrett, C. J. R., and W. H. Munk, 1972: Space–time scales of internal waves. *Geophys. Fluid Dyn.*, **3**, 225–235.

——, ——, 1975: Space–time scales of internal waves: A progress report. *J. Geophys. Res.*, **80**, 291–297.

Gossard, E. E., and W. H. Hooke, 1975: *Waves in the Atmosphere.* Elsevier.

Hines, C. O., 1960: Internal gravity waves at ionospheric heights. *Can J. Phys.*, **38**, 1441–1481.

——, 1974: *The Upper Atmosphere in Motion, Geophys. Monogr.*, No. 18, Amer. Geophys. Union

Houghton, J. T., 1978: The stratosphere and mesosphere. *Quart. J. Roy. Meteor. Soc.*, **104**, 1–29.

Lindzen, R. S., 1981: Turbulence and stress owing to gravity wave and tidal breakdown. *J. Geophys. Res.*, **86**, 9707–9714.

Manson, A. H., and C. E. Meek, 1988: Gravity wave propagation characteristics (60–120 km) as determined by the Saskatoon MF radar (Gravnet) system: 1983–85 at 52°N, 107°W. *J. Atmos. Sci.*, **45**, 932–946.

Meek, C. E., I. M. Reid and A. H. Manson, 1985a: Observation of mesospheric wind velocities, 1. Gravity wave horizontal scales and phase velocities determined from spaced wind observations. *Radio Sci.*, **20**, 1363–1382.

——, —— and ——, 1985b: Observation of mesospheric wind velocities, 2. Cross sections of power spectral density for 48-8 hours, 8-1 hours, and 1 hour to 10 min. over 60–110 km for 1981. *Radio Sci.*, **20**, 1383–1402.

Palmer, T. N., G. J. Shutts and R. Swinbank, 1986: Alleviation of a systematic westerly bias in general circulation and numerical weather prediction models through an orographic gravity wave drag parameterization. *Quart. J. Roy. Meteor. Soc.*, **112**, 1001–1040.

Pinkel, R., 1981: On the use of Doppler sonar for internal wave measurements. *Deep-Sea Res.*, **28A**, 269–289.

Reid, I. M., and R. A. Vincent, 1987: Measurements of mesospheric gravity wave momentum fluxes and mean flow accelerations at Adelaide, Australia. *J. Atmos. Terr. Phys.*, **49**, 443–468.

Scheffler, A. O., and C. H. Liu, 1988: The effects of Doppler shift on the gravity wave spectra observed by MST radar. *J. Atmos. Terr. Phys.*, **48**, 1225–1231.

VanZandt, T. E., 1982: A universal spectrum of buoyancy waves in the atmosphere. *Geophys. Res. Lett.*, **9**, 575–578.

——, 1985: A model for gravity wave spectra observed by Doppler sounding systems. *Radio Sci.*, **20**, 1323–1330.

Vincent, R. A., and I. M. Reid, 1983: HF Doppler measurements of mesospheric momentum fluxes. *J. Atmos. Sci.*, **40**, 1321–1333.

——, and D. C. Fritts, 1987: A climatology of gravity wave motions in the mesopause region at Adelaide, Australia. *J. Atmos. Sci.*, **44**, 748–760.